IJMSO

International Journal of Mathematical Sciences and Optimization: Theory and Applications
12(1), 2026, Pages 91 - 103
https://doi.org/10.5281/zenodo.20467141

Dissipative Hydromagnetic Flow of an Arrhenius Fluid with Variable Properties under No-Slip Boundary Conditions

A. Adeniyan[1], S. A. Odunlami[2], E. O. Fatunmbi [3*]

1. Mathematics/Statistics Units, Trinity University, Yaba Lagos, Nigeria.
2. Department of Mechanical Engineering, Federal Polytechnic Ilaro, Nigeria.
3. Department of Mathematics and Statistics, Federal Polytechnic Ilaro, Nigeria.
Email: [1]tunjadeniyan@yahoo.com, [2]samson.odunlami@federalpolyilaro.edu.ng
* Corresponding author: ephesus.fatunmbi@federalpolyilaro.edu.ng

Article Info
Received: 25 February 2026 Revised: 22 March 2026
Accepted: 25 March 2026 Available online: 15 April 2026

Abstract

This study focuses on investigating the non-slip hydromagnetic laminar dissipation flow with Arrhenius kinetics in binary reactions characterized by reaction order and variable properties within an unbounded isothermal device. In the absence of material distortion, the species mixture in the fluid is activated by factors such as internal heating, reaction order, and activation energy. This study focuses on investigating the non-slip hydromagnetic laminar dissipation flow with Arrhenius kinetics in binary reactions characterized by reaction order and variable properties within an unbounded isothermal device. In the absence of material distortion, the species mixture in the fluid is activated by factors such as internal heating, reaction order, and activation energy. The partial differentiation model is nondimensionalized to a thermofluidic dimensionless form. An invariant quasi-linear coupled ordinary differentiation model is obtained using appropriate similarity quantities. Computation solutions of the dimensionless invariant formulated derivative model are offered in plots and tabular formats to illustrate the sensitivity of critical terms. The analysis reveals that the species mixture leads to a reduction in flow velocity but an increase in binary species reaction by 0.734%. Furthermore, the activation energy and coefficient material enhance the thermic profile within the flow medium. Consequently, this study provides valuable insights for industrial development, aiding in the informed selection of working fluid properties.

Keywords: No-slip condition; Activation energy; Reaction order; Arrhenius kinetics; Viscous Dissipation.
MSC2010: 35Q20.

IJMSO

International Journal of Mathematical Sciences and Optimization: Theory and Applications
12(1), 2026, Pages 91 - 103
https://doi.org/10.5281/zenodo.20467141

Nomenclature

Symbol	Description
K_T	Variable thermal conductivity
k	Uniform thermal conductivity
u, v	Velocities in x and y directions
$C(T)$	Fluid concentration(temperature)
D	Species diffusion coefficient
R	Reynolds number
U	Velocity of the free stream
$C_\infty(T_\infty)$	free stream concentration (temperature)
H	Hartmann number
c_p	Specific heat at constant pressure
k_r	Boundary wall chemical reaction parameter
q_w	Boundary wall surface heat flux
E_a	Activation energy
R_G	Universal gas constant
g	Gravitational acceleration
r	Positive integer
Dimensionless Groups	
Gr	Grashof number
N	Buoyancy ratio parameter
Fs	Darcy–Forchheimer parameter
V	Limiting velocity
$Sc(Pr)$	Schmidt (Prandtl)number
Greek Letters	
$\theta(\phi$	Dimensionless temperature(concentration)
β	viscous dissipation parameter
$\beta_c(\beta_T)$	Species (thermal) expansion coefficient
ϵ	Dimensionless activation energy
$\chi(\tau)$	chemical reaction (thermal diffusion) parameter
λ	Binary chemical reaction parameter
ϵ	Small positive parameter $(0 < \epsilon \ll 1)$
$\alpha_0(\alpha_1)$	heat source/sink (wall heating) term

1 Introduction

The flow of current-carrying fluid materials stimulated by magnetic force is presently given much attention owing to its usage in MHD generators, heat conductors, oil exploration, fusion and fission reactions, plasma, and so on [1, 2]. The magnetic-induced flowing fluid was reported to have supported the efficiency of industrial lubricant viscosity due to the impact of electromagnetic force that damped free flow and its ability to conduct heat away from a system [3, 4]. Several extensive researches have been performed on different magnetohydromagnetic fluid flow models in various geometries. Khan et al. [5] examined the dual solution of magneto-nanomaterial on a curved surface. The flow rate was reported to have been damped with rising magnetic terms. Ahmed et al. [6] considered the thermo-physical impact of magnetic force on a nanofluid flow past a Couette horizontal device. It was found that magnetic force retarded the flow near the fixed surface. Nadeem et al. [7] considered magnetic viscous flow in a vertical configuration and reported that material properties supported the magnetic force in opposing the flow and increased fluid viscosity. Oyeyinka et al. [8] analytically investigated the flow of MHD Williamson fluid past inclined elongated device embedded in porous medium subject to mixed convection and heat generation. Fatunmbi et al. [9] examined the stagnation point flow of an electrically conducting Williamson nanofluid over an expanding

IJMSO

International Journal of Mathematical Sciences and Optimization: Theory and Applications
12(1), 2026, Pages 91 - 103
https://doi.org/10.5281/zenodo.20467141

device in the presence of Ohmic heating and entropy analysis, whereas Adigun et al. [10] analyzed the flow of MHD tangent hyperbolic stratified fluid over a vertically stretched with quadratic mixed convection and nonlinear thermal radiation effects. Nmeburulo et al. [11] discussed on heat-mass transfer of steady hydromagnetic boundary layer flow past a non-permeable flat sheet with Ohmic and viscous heating effects. The authors reported there is a decrease in the fluid velocity but a rise in the temperature as the magnetic parameter increases in strength.

Meanwhile, many industrial and technological processes for reacting species involving hydromagnetic flow are often accompanied by heat transfer [12]. As such, Rahman [13] examined nanofluid exothermic species reaction in the porous cavity with a sloping magnetic field and heat transfer. It was presented that heat transfer is enhanced with a rising exothermic reaction, which reduces fluid viscosity. Khan et al. [14] theoretically examined the Maxwell mixed convective flow in an isothermal infinite stretchable disk with heat generation/sink. The findings show that the heat generation enhanced heat propagation and chemical reaction. In a vertical device, Nadeem [15] examined the heat transport of chemically reacting hydromagnetic nanomaterial in a Maxwell base fluid with a heat sink. The magnetic field is seen to have increased heat transfer but damped the reacting fluid flow velocity. In practical phenomena, differences in the species concentration mixture led to mass transfer, which is useful in many industrial and chemical mixtures [16, 17]. Every reacting species requires a minimum energy to stimulate the reaction.

The mechanism for reacting species of mass diffusion influenced by Arrhenius activation energy is often encountered in oil and water emulsions, food processing, chemical engineering, thermal reservoirs, and so on [18]. No matter how small, fluid molecular reaction requires potential and kinetic energies for the Arrhenius chemical mixture, but as a result of pronounced momentum energy, small activation energy may be needed to break the molecular bond [19]. The significance of the activation energy concept can be found in geothermal processes, oil industries, hydromagnetic processes, oil suspension, and others. Owing to its usefulness Acharya et al. [20] presented a binary chemical mixture and reduction of entropy generation in Arrhenius activation energy of radiative hydromagnetic nanomaterial flow past a vertical plate. It was stated that temperature field and thermal diffusion are enhanced with rising radiation variables. Azama et al. [21] investigated the nanofluid covalent bonding of cross-radiation in an axisymmetric flow with the Arrhenius activation energy effect. The numerical outcomes depicted that the chemical concentration profile is raised with high activation energy. Mustafa et al. [22] investigated the influence of activation energy and buoyancy force on hydromagnetic chemically reacting nanofluid flow in a vertical medium. The numerical study shows that nanofluid concentration rises proportional to the Arrhenius chemical reaction rate. In ref. [23], the authors presented the entropy generation of an Oldroyd 8-constant hydromagnetic fluid in a double Arrhenius reaction and current density. From the analytical results, it was stated that the second exothermic reaction term enhances reaction combustion. Other investigations on the Arrhenius activation energy for different fluid materials can be found in [24–28].

This study focuses on the influence of varying heat generation, heat dissipation, and activation energy on a hydromagnetic heat transfer and chemical reaction occurring in an isothermal vertical device. The study is significant in chemical sciences, industrial processes, engineering, etc. Of many related studies or models, no combined effect of magnetic field, activation energy, varying heat source, and thermal dissipation have been examined despite their significance in many aspects of sciences and engineering. Hence, the usefulness of this study to the thermal chemical sciences motivated the interest. As such, the investigation is inspired by the phenomenal applications of the study coupled with the significant reports from various researchers as seen in [12, 15, 18, 22]. A numerical analysis of the model is carried out using a shooting method combined with the Runge-Kutta scheme; the outcomes are given in tables and graphs and qualitatively discussed.

2 Problem Formulation and Modelling

A theoretical non-slip hydromagnetic laminar flow of chemical reacting fluid in a vertical boundless device is considered. The flow is influenced by viscous dissipation, varying heat sources, pressure

IJMSO

International Journal of Mathematical Sciences and Optimization: Theory and Applications
12(1), 2026, Pages 91 - 103
https://doi.org/10.5281/zenodo.20467141

gradient, and temperature-dependent thermal conductivity without reacting material species consumption. The fluid particles collided continuously without deformation, satisfying Newtons law of flow motion. The fluid chemical reaction is stimulated by branched reaction order, activation energy, internal heating, and chemical kinetics. The magnetic field controls the fluid conductivity strength at low Reynolds numbers with negligible magnetic induction. The boundary layer flow equations are formulated based on the highlighted assumptions, which follow from the recent works of [29, 30]. Hence, the velocity component, energy, and mass equations, as well as the boundary conditions governing the flow, are given as:

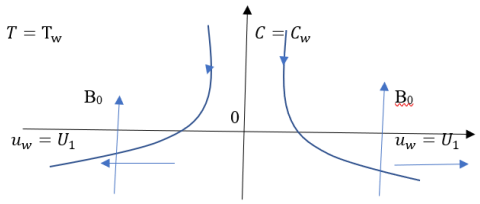

Figure 1: Flow Configuration

2.1 Governing Equations

Incorporating the above-highlighted assumptions, the relevant governing equations for the momentum, microrotation, energy, and concentration equations are expressed as follow. The governing equations for the flow are given as:

$$u\frac{\partial u}{\partial x}+v\frac{\partial u}{\partial y}=-\frac{1}{\rho}\frac{\partial p}{\partial x}+\nu\left(\frac{\partial^2 u}{\partial x^2}+\frac{\partial^2 u}{\partial y^2}\right)-\frac{\sigma B^2(x)}{\rho}(u-U)\mp g\frac{K_1}{\nu}|u|(u-U)+g\left[\beta_T(T-T_\infty)+\beta_C(C-C_\infty)\right], \tag{2.1}$$

$$u\frac{\partial v}{\partial x}+v\frac{\partial v}{\partial y}=-\frac{1}{\rho}\frac{\partial p}{\partial y}+\nu\left(\frac{\partial^2 v}{\partial x^2}+\frac{\partial^2 v}{\partial y^2}\right)-\frac{\sigma B^2(x)}{\rho}v, \tag{2.2}$$

$$\rho c_p\left(u\frac{\partial T}{\partial x}+v\frac{\partial T}{\partial y}\right)=\frac{\partial}{\partial y}\left(k\frac{T}{T_\infty}\frac{\partial T}{\partial y}\right)+\mu\left(\frac{\partial u}{\partial y}\right)^2-\frac{ku_w(x)}{x\nu}\left[A^*(T_w-T_\infty)(u-U)+B^*(T-T_\infty)\right], \tag{2.3}$$

$$\rho\left(u\frac{\partial C}{\partial x}+v\frac{\partial C}{\partial y}\right)=D\frac{\partial^2 C}{\partial y^2}+\gamma(C-C_\infty)-k_r^2(T-T_\infty)^r\exp\left(-\frac{E_a}{R_G T}\right)(C-C_\infty). \tag{2.4}$$

The model is subjected to boundary conditions:

$$\begin{cases} u=U_1, v=v_w, T=T_w, C=C_w \text{at } y=0 \\ u\to U, T\to T_\infty, C\to C_\infty \text{as } y\to\infty. \end{cases} \tag{2.5}$$

2.2 Non-Dimensional Variables

The following appropriate variables are applied to the system of flow dimensional equations to obtain dimensionless transformed equations as demonstrated by [21, 24]

$$\begin{cases} x'=\frac{x}{L}, y'=\frac{y}{\delta}, u'=\frac{u}{U}, v'=\frac{vL}{U\delta}, \\ p'=\frac{p}{\rho U^2}, U'=\frac{U}{U_0}, (T-T_\infty)=\theta\left(\frac{E_a}{R_G T_\infty^2}\right)^{-1} \\ \phi=\frac{C-C_\infty}{C_w-C_\infty}, V=\frac{U_1}{U_0}, \omega'=\frac{4}{v_0^2} \end{cases} \tag{2.6}$$

where L is scale length, δ is the unknown thickness of the device layer for which $x=L$, U is the velocity of the flowing liquid along the x-axis parallel to the bounded flow medium layer. Now, using the defined quantities of equations (2.6) on the formulated flow boundary equations (2.1) to

IJMSO

International Journal of Mathematical Sciences and Optimization: Theory and Applications
12(1), 2026, Pages 91 - 103
https://doi.org/10.5281/zenodo.20467141

(2.5), the non-dimensional flow system of equations without the prime is obtained as in the limit $R \to$:

$$\frac{\partial u}{\partial x} + \frac{\partial v}{\partial y} = 0 \tag{2.7}$$

$$u\frac{\partial u}{\partial x} + v\frac{\partial u}{\partial y} = G(x) + \frac{\partial^2 u}{\partial y^2} - H(u-1) \mp F_s(u-1) + Gr(N\theta + \phi), \tag{2.8}$$

$$u\frac{\partial \theta}{\partial x} + v\frac{\partial \theta}{\partial y} = \tau\frac{\partial}{\partial y}\left[(1+\varepsilon\theta)\frac{\partial \theta}{\partial y}\right] + \beta\left(\frac{\partial u}{\partial y}\right)^2 - \alpha_0\left[\alpha_1(u-1) + \theta\right], \tag{2.9}$$

$$u\frac{\partial \phi}{\partial x} + v\frac{\partial \phi}{\partial y} = \frac{1}{Sc}\frac{\partial^2 \phi}{\partial y^2} + \chi\phi - \varepsilon\lambda\theta^r \exp\left(\frac{\theta}{1+\varepsilon\theta}\right)\phi. \tag{2.10}$$

Dimensionless Boundary Conditions

$$\begin{cases} u = V, v = 0, \theta = 1, \phi = 1 \text{at} \quad y = 0 \\ u \to 1, \theta \to 0, \phi \to 0 \text{as } y \to \infty \end{cases} \tag{2.11}$$

The thermo-fluid physical parameters are defined as:

$$\begin{aligned} &H = \frac{\sigma\mu B^2(x)L}{kU}, Gr = \frac{g\beta_c(C_w - C_\infty)L}{U^2}, N = \frac{\beta_T R_G T_\infty^2 L}{\beta_c E_a (C_w - C_\infty)U^2}, F_s = g\frac{K_1}{\nu}\frac{L}{U}|u|, \\ &\tau = \frac{k}{\mu c_p}\frac{L}{U\delta^2 T_\infty}, \varepsilon = \frac{R_G T_\infty}{E_a}, \beta = \frac{\rho U^3 L}{\delta^2}\frac{E_a}{R_G T_\infty^2}, \chi = \frac{2x\gamma L}{\rho U^2}, \alpha_1 = \frac{A^*(T_w - T_\infty)E_a U}{B^* b x R_G T_\infty^2}, \\ &\alpha_0 = \frac{LB^*}{U}\left(\frac{\kappa u_w(x)}{x\nu}\right), \lambda = k_r^2\frac{2xL}{\rho U^2}(\varepsilon T_\infty)^r \exp\left(-\frac{1}{\varepsilon}\right), \frac{1}{Sc} = \frac{DL}{\mu U}, R = \frac{UL}{\nu}. \end{aligned} \tag{2.12}$$

For the flow velocity U parallel to the flat vertical plate, the pressure is independent of y. At the leading edge $(x = 0, y = 0)$, the velocity gradient becomes indefinite, indicating the presence of a mathematical singularity. Consequently, the boundary layer approximation is not valid exactly at the leading edge but remains valid in the vicinity of $x \approx 0$. Thus, the boundary layer equations (2.7)–(2.11) can be reduced to a system of ordinary differential equations using an appropriate similarity transformation. A one-parameter transformation is introduced such that the governing equations become invariant. The stream function ψ is defined as:

$$\begin{cases} \psi = \sqrt{2\nu U x}\, f(\eta), \eta = \sqrt{\frac{U}{2\nu x}}\, y, u = \frac{\partial \psi}{\partial y} = U f'(\eta), \\ v = -\frac{\partial \psi}{\partial x} = \sqrt{\frac{U\nu}{2x}}\left(\eta f'(\eta) - f(\eta)\right), \\ \frac{\partial \eta}{\partial x} = -\frac{\eta}{2x}, \frac{\partial \eta}{\partial y} = \sqrt{\frac{U}{2\nu x}}. \end{cases} \tag{2.13}$$

Substituting equation (2.13) into the governing equations, the continuity equation is identically satisfied. The momentum, energy, and species equations reduce to:

$$f''' + ff'' - (H \pm F_s)(f' - 1) + Gr(N\theta + \phi) + G = 0 \tag{2.14}$$

$$\tau\left[(1+\varepsilon\theta)\theta'\right]' + f\theta' + \beta(f'')^2 - \alpha_0\left[\alpha_1(f'-1) + \theta\right] = 0 \tag{2.15}$$

$$\frac{1}{Sc}\phi'' + f\phi' + \chi\phi - \lambda\theta^r \exp\left(\frac{\theta}{1+\varepsilon\theta}\right)\phi = 0 \tag{2.16}$$

The transformed boundary conditions are:

$$\begin{cases} f(0) = 0, \quad f'(0) = V, \quad \theta(0) = 1, \quad \phi(0) = 1 \\ f'(\eta) \to 1, \quad \theta(\eta) \to 0, \quad \phi(\eta) \to 0 \text{as } \eta \to \infty \end{cases} \tag{2.17}$$

IJMSO

International Journal of Mathematical Sciences and Optimization: Theory and Applications
12(1), 2026, Pages 91 - 103
https://doi.org/10.5281/zenodo.20467141

In the absence of external forces and thermal effects, the momentum equation reduces to:

$$f''' + ff'' = 0 \tag{2.18}$$

The numerical solution gives: $f''(0) = 0.469599998500248$. The point solution is presented in Figure 2.

2.3 Engineering Quantities of Interest

The physically important quantities are the skin friction coefficient, Nusselt number, and Sherwood number, defined respectively as:

$$\begin{cases} C_f = f''(0), \\ Nu = -\theta'(0), \\ Sh = -\phi'(0) \end{cases} \tag{2.19}$$

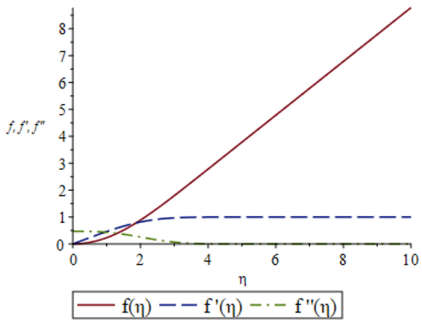

Figure 2: A one-parameter functions f(),f'() and f"().

The range of values at the horizontal axis is denoted by η. In contrast, the functions $f(), f'()$ and $f''()$ are considered on the vertical axis as presented in Figure 2. The numerical point solutions for the flow field, velocity field, and wall velocity gradient are demonstrated in the plot.

3 Numerical Computation Technique

The transformed nonlinear ordinary differential equations (2.14)–(2.16), together with boundary conditions (17), are solved numerically over the domain $0 < \eta < \eta_\infty$. A finite computational domain is adopted with $\eta_\infty = 5$, which is sufficient to satisfy the asymptotic boundary conditions. The domain is discretized using a uniform step size of $\Delta\eta = 0.02$, ensuring accuracy and convergence. The computations are carried out using *Maple 2020*. The chosen parameter values are: $\varepsilon = N = \lambda = G = 0.1, Pr = 7.0, Sc = 0.6, V = F_s = H = 0.2, \beta = 0.04, Gr = 0.5, \alpha_0 = 0.02, \alpha_1 = 0.05, r = 1.0$. These values are selected based on existing literature.

4 Results and Discussion

In Table 1, the results of the present study are compared with the previous ones to check the accuracy of the numerical computations. The comparison shows good agreement between the present results and existing results in the literature for skin friction and Nusselt number as Pr and Sc vary in magnitude. Also, the numerical results for skin friction $f''(0)$, heat transfer rate $-\theta'(0)$, and mass transfer rate $-\phi'(0)$ are presented in Table 2 for variation in α_0, χ, G, H, N and Gr. The table shows the sensitivity of the chemical reacting fluid and temperature to parameter variation. As such, these parameters should be monitored for the effective usage of various working fluids to enhance their performance.

IJMSO

International Journal of Mathematical Sciences and Optimization: Theory and Applications
12(1), 2026, Pages 91 - 103
https://doi.org/10.5281/zenodo.20467141

Table 1: Results verification with existing related studies

Parameters		**Makinde [31]**		**Okedoye et al. [29]**		**Present results**	
Pr	Sc	C_f	Nu	C_f	Nu	C_f	Nu
0.50	0.71	3.09046	1.21628	3.09048	1.21627	3.09035	1.21657
0.70	0.71	2.77995	1.21263	2.77998	1.21262	2.78003	1.21239
0.60	1.00	2.79576	1.49400	2.79577	1.49399	2.79568	1.49410
0.60	5.00	1.75935	4.36421	1.75937	4.36421	1.75948	4.36457

From the Table 2, it is noted that an increase in G, and H implies a greater Lorentz force that opposes fluid motion, thereby enhancing shear stress on the wall. A rise in χ results in greater wall shear force and improved heat and mass transfer performance. The reaction rate increases when χ value rises which leads to greater species consumption or generation that occurs close to the wall. The local gradients in velocity and temperature and concentration increase which results in higher values for $f''(0), -\theta'(0)$ and $(-\phi'(0))$. The trend shows that chemical reactions enhance boundary-layer flow and promote better momentum and thermal and mass transfer at the surface. Similarly, an increase in Gr implies an increase in buoyancy force, which accelerates fluid flow near the surface, thereby enhancing the velocity gradient, which in turn increases skin friction. On the contrary, an increase in α_0 implies a decrease in fluid viscosity, thereby decreasing shear stress on the wall.

Table 2: Effect of α_0, χ, G, H, N and Gr on skin friction, temperature and mass gradient

α_0	χ	G	H	N	Gr	$f''(0)$	$-\phi'(0)$	$-\theta'(0)$
0						1.1285264	-0.5077929	-0.5139627
0.2						1.1265668	-0.5072815	-0.6078117
0.4						1.1249422	-0.5068625	-0.6910885
1.0						1.1213691	-0.5059558	-0.8990935
	0.0					1.0626547	-0.8994555	-0.5172553
	0.5					1.0886094	-0.7319737	-0.5198783
	1.0					1.2623458	0.1043590	-0.5372888
	3.0					1.7512308	2.0775658	-0.5768939
		0.0				0.9799411	-0.4876214	-0.5075284
		0.5				1.6910721	-0.5724704	-0.5720068
		1.0				2.3456045	-0.6329471	-0.6082391
		3.0				4.6745359	-0.7876058	-0.6375864
			0.0			1.0774817	-0.5066292	-0.5229433
			0.4			1.1784640	-0.5089507	-0.5249500
			1.2			1.3684251	-0.5140091	-0.5290248
			2.0			1.5404663	-0.5186606	-0.5325403
				0.0		1.0947979	-0.5050664	-0.5217401
				0.5		1.2598287	-0.5179152	-0.5320689
				1.0		1.4191753	-0.5296643	-0.5411629
				1.5		1.5737389	-0.5405211	-0.5492400
					0.0	0.7287420	-0.4724569	-0.4940437
					1.0	1.4913757	-0.5355235	-0.5455688
					3.0	2.7548605	-0.6132785	-0.5935911
					5.0	3.8569849	-0.6668174	-0.6115227

A rise in α_0, G, H, N, and Gr enhances heat transfer due to an improvement in thermal transport mechanisms. An increase in Gr and N implies an increase in buoyancy-driven convection, which accelerates thermal mixing, thereby enhancing the temperature gradient on the wall. Similarly, an increase in H implies an increase in the magnetic field, which may accelerate thermal energy

IJMSO
International Journal of Mathematical Sciences and Optimization: Theory and Applications
12(1), 2026, Pages 91 - 103
https://doi.org/10.5281/zenodo.20467141

transport via Joule heating. However, an increase in χ implies a decrease in heat transfer due to the suppression of fluid motion caused by increased fluid resistance within the porous material.It is observed that the skin friction coefficient increases with increasing values of χ, G, H, N and Gr, but decreases as α_0 increases. Similarly, the rate of heat transfer enhances with increasing α_0, G, H, N and Gr, whereas it decreases with increasing χ. The mass transfer rate improves as α_0, χ, G, H, N and Gr increase. This improvement is linked to enhanced mass transport. Stronger buoyancy effects (Gr, N) and flow resistance parameters modify the concentration boundary layer, leading to steeper concentration gradients at the wall. This results in an increased rate of species diffusion from the surface.

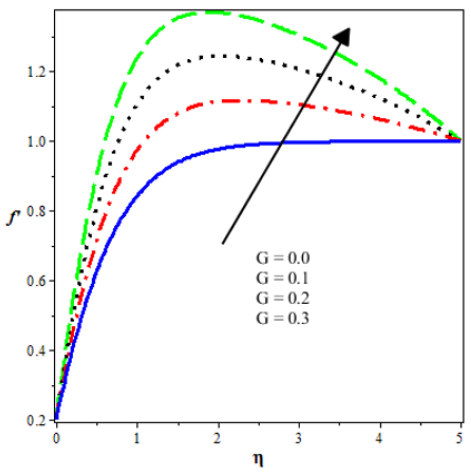

Figure 3: Velocity curve pattern for varying G

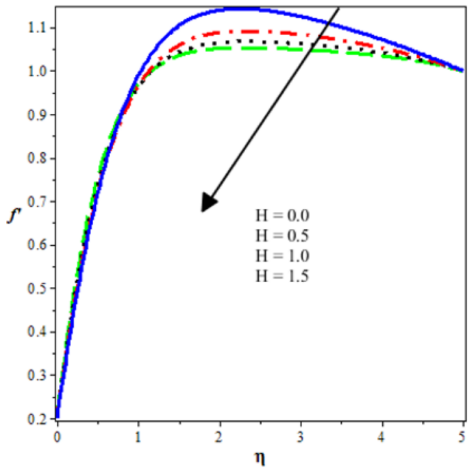

Figure 4: Velocity profile for rising H

Figure 3 shows that an increase in the pressure gradient parameter G enhances the velocity profile due to increased driving force. A favourable pressure gradient creates a driving force that accelerates fluid motion while increasing its kinetic energy. Also, the boundary layer momentum increase results in elevated velocity profiles. Whereas in Figure 4, the Hartmann number stimulated electromagnetic force (Lorentz force) to drag the velocity distribution near the bounded plate, the flow velocity is propelled along the stream due to rising vary heat generation.

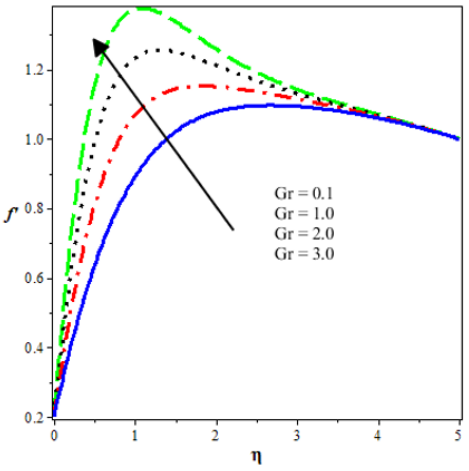

Figure 5: Velocity curve pattern for varying Gr

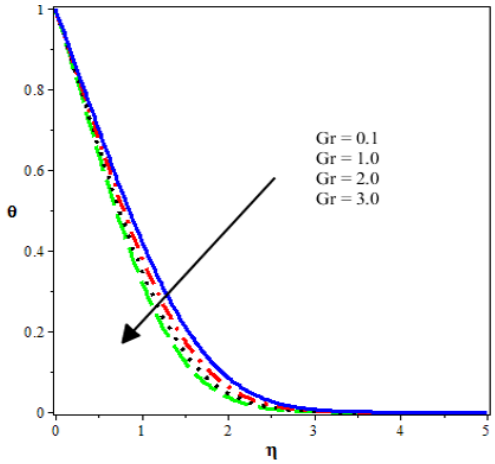

Figure 6: Thermal profile for rising Gr

The electromagnetic force dominates the viscous fluid, which declines the conducting fluid velocity profile past a magnetic field near the plate. Also, the rising Grashof number encourages the flow velocity profile, as noticed in Figure 5. The approximated fluid buoyancy force ratio dominates

IJMSO
International Journal of Mathematical Sciences and Optimization: Theory and Applications
12(1), 2026, Pages 91 - 103
https://doi.org/10.5281/zenodo.20467141

the exerting viscous force to stimulate natural convection; this leads to a significant rise in flow rate magnitude. A rise in temperature change has been influenced by reducing changes in the fluid density resulting in an enhancing velocity field.

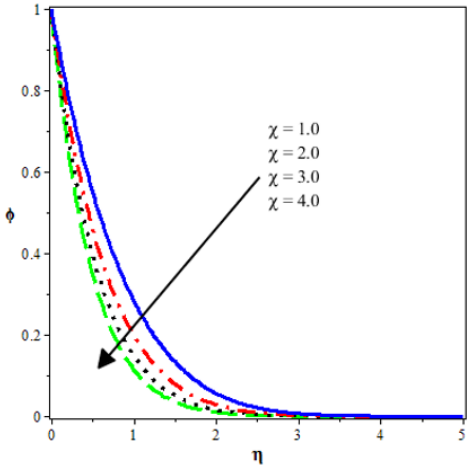

Figure 7: Concentration distribution for rising χ

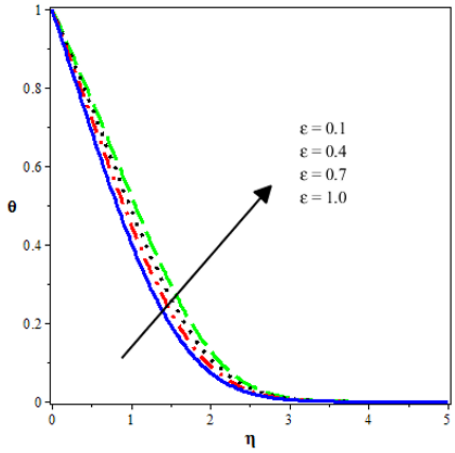

Figure 8: Velocity profile for variation in

However, in Figure 6, the Grashof number (Gr) decreases the heat transfer field due to the strong influence of viscous force that discouraged free liquid particle interaction. As well, the fluid density increases to damp the increasing changes in temperature, as a result, the temperature profile magnitude is reduced. Figures 7 demonstrates the chemical reaction effect χ on the reaction species transfer. Figure 7 illustrate the graph of the concentration profile as χ rises in magnitude. In this plot, growth in the chemical reaction parameter boosts the consumption of the species within the boundary layer, and thus leads to a faster depletion of concentration near the surface, which consequently decreases the concentration across the fluid. However, a rise in the dimensionless activation energy propels an increase in the thermal field as noted in Figure 8. This is because a rise in reduces the effective activation barrier,and enhancing the chemical reaction rate. This generates additional heat within the boundary layer, causing the temperature profile the temperature profile to rise and increasing thermal energy throughout the fluid.

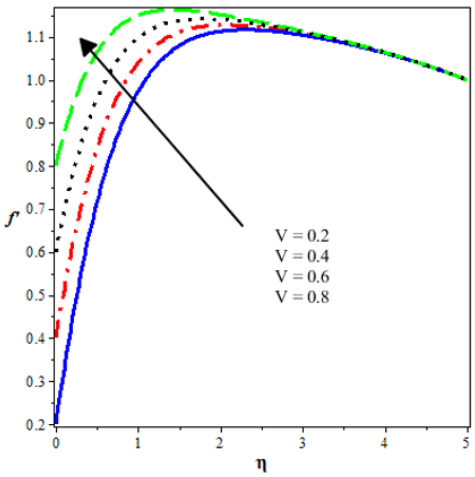

Figure 9: Flow rate profile for increasing (V)

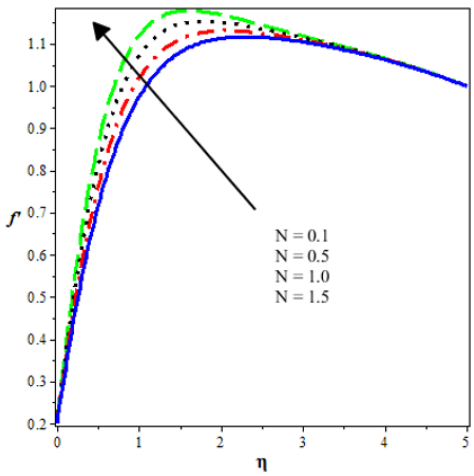

Figure 10: Velocity field for different N

The inspired heat dispersion propels the chemical reaction rate, leading to species-molecular interaction, thereby encouraging the flow rate and concentration distribution. Figures 9 and 10 show that the limiting velocity (V) and the buoyancy ratio (N) increase the laminar Newtonian flow

IJMSO
International Journal of Mathematical Sciences and Optimization: Theory and Applications
12(1), 2026, Pages 91 - 103
https://doi.org/10.5281/zenodo.20467141

velocity profile. A solid continuous rise in the velocity filed along the bounded stream is seen; due to the dominance of heat generation over the fluid viscosity. As such, the molecular bond is reduced to enhance the fluid material mixture, and caused the flow dimension to be raised. This is found to have been aligned with various existing reports from the literature (see refs. [5, 6]).

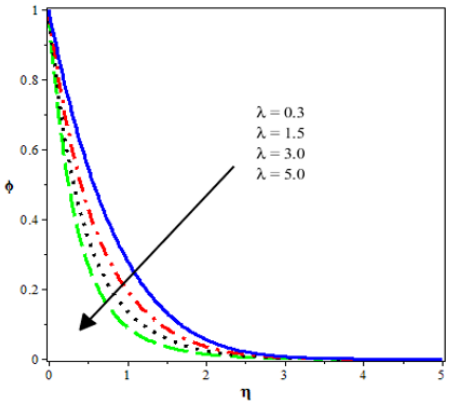

Figure 11: The λ on velocity profile

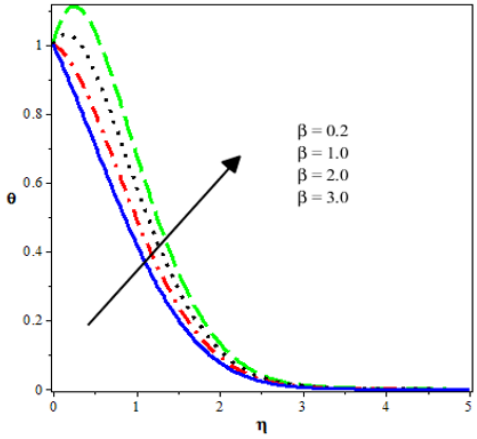

Figure 12: Thermal profile for rising Gr

The impact of the binary reacting mixture term λ on the concentration diffusion is illustrated in Figure 11. The binary reaction parameter λ suppresses both concentration due to increased molecular interactions. Furthermore, a rise λ corresponds to growth in the temperature-dependent chemical reaction rate, leading to faster consumption of the species. As a result, there is a rise in species depletion within the boundary layer, leading to a decline in the concentration profile across the fluid. Figure 12 reveals the effect of the viscous dissipation parameter β on the thermal profile. This parameter amplifies the conversion of kinetic energy into thermal energy due to internal fluid friction, thus it causes the temperature profile to elevate as seen in the figure. . This effect is particularly significant in high-speed or highly viscous flows, including polymer extrusion, lubricated mechanical systems, or nanofluid-based solar collectors, etc., where viscous heating can enhance heat transfer rates, improve thermal efficiency, and influence chemical reaction rates within the working fluid.

5 Conclusion

A numerical investigation of the continuous non-slip flow of hydromagnetic Arrhenius kinetics fluid reaction with thermal conductivity and heat generation variable properties is carried out in a vertical medium. The flow characteristics of the thermo-fluid entrenched parameters and the reactive species diffusion rate sensitivity are established numerically. The behaviour of the Arrhenius reactive kinetics fluid along the bounded plate surface is presented in tables for various fluid physical terms. The observation made from the study depicted that:

- Increasing the magnitude of V, G, N, and Gr enhances both the velocity profiles, raises heat transfer, and species diffusion due to stronger driving forces, and buoyancy effects. The skin friction coefficient rises with χ, G, H, N, and Gr, but decreases with α_0.
- The intensity of the thermal profile rises as β and *epsilon* increase in magnitude. These parameters encourage internal heat generation and facilitate the Arrhenius reaction, and elevating thermal energy across the boundary layer. On the other hand, the thermal profile declines with growth in Gr but raises the heat transfer due to viscous damping of thermal convection.
- There is a decline in the concentration profile as χ and λ elevate in the system. The trend indicates a higher chemical reaction rates and species consumption.

- The combination of buoyancy (Gr, N), magnetic field (H), and pressure gradient (G) affect the momentum distribution. Higher electromagnetic forces lower the velocity because of the Lorentz drag but pressure gradients and buoyancy propel flow acceleration and momentum boundary-layer thickness.

The results of this study provide essential benefits for lubricant oil production and polymer extrusion and synthetic chemical processes and nanofluid-based thermal systems which require process control to achieve higher operational efficiency and productivity. The framework can be extended to viscoelastic fluids or flows in annular and concentric geometries for industrial applications.

References

[1] Acharya N. (2021). Spectral quasi linearization simulation on the radiative nanofluid spraying over a permeable inclined spinning disk considering the existence of heat source/sink. Applied Mathematics and Computation, 411, 126547.

[2] Bera T. K., Bohre A. K., Ahmed I., Bhattacharya A., & Bhowmik P. S. (2022). Magnetohydrodynamic (MHD) power generation systems. In Planning of hybrid renewable energy systems, electric vehicles and microgrid: Modeling, control and optimization (pp. 905–929). Springer Nature Singapore.

[3] Fatunmbi E. O., & Okoya S. S. (2020). Heat transfer in boundary layer magneto-micropolar fluids with temperature-dependent material properties over a stretching sheet. Advances in Materials Science and Engineering, 20, 1–11.

[4] Reddy M. G., Kumar N., Prasannakumara B. C., Rudraswamy N. G., & Kumar K. G. (2021). Magnetohydrodynamic flow and heat transfer of a hybrid nanofluid over a rotating disk by considering Arrhenius energy. Communications in Theoretical Physics, 73, 045002.

[5] Khan A. U., Hussain S. T., & Nadeem S. (2019). Existence and stability of heat and fluid flow in the presence of nanoparticles along a curved surface by means of dual nature solution. Applied Mathematics and Computation, 353, 66–81.

[6] Ahmed Z., Al-Qahtani A., Nadeem S., & Saleem S. (2019). Computational study of MHD nanofluid flow possessing micro-rotational inertia over a curved surface with variable thermophysical properties. Processes, 7, 387–394.

[7] Nadeem S., Khan M. R., & Khan A. U. (2019). MHD stagnation point flow of viscous nanofluid over a curved surface. Physica Scripta, 94, 115207.

[8] Oyeyinka T. A., Oderinu R. A., Alao S., Sanusi B. A., & Ayanbukola F. J. (2025). An analytical investigation of MHD Williamson fluid flow over an inclined stretching sheet in a porous medium with non-uniform internal heat generation and mixed convection. International Journal of Mathematical Sciences and Optimization: Theory and Applications, 11(4), 123–137.

[9] Fatunmbi E. O., Mabood F., & Adeniyan A. (2021). Stagnation-point flow of magneto-Williamson nanofluid over a stretching material with Ohmic heating and entropy analysis. International Journal of Mathematical Sciences and Optimization: Theory and Applications, 7(1), 131–145.

[10] Adigun A. J., Fatunmbi E. O., & Boneze C. U. (2022). Quadratic mixed convection tangent hyperbolic stratified fluid flow past a vertical elongated sheet with nonlinear thermal radiation: Spectral local linearization method. International Journal of Mathematical Sciences and Optimization: Theory and Applications, 8(2), 131–148.

[11] Nmeburulo I. E., Durojaye M. O., & Ajie J. I. (2023). Modelling the effects of heat and mass transfer on steady two-dimensional hydromagnetic flow over an impermeable surface. International Journal of Mathematical Sciences and Optimization: Theory and Applications, 9(2), 53–61.

[12] Salawu S. O., & Dada M. S. (2018). Lie group analysis of Soret and Dufour effects on radiative inclined magnetic pressure-driven flow past a Darcy–Forchheimer medium. Journal of Serbian Society for Computational Mechanics, 12, 108–125.

[13] Rahman M. M., Pop I., & Saghir M. Z. (2019). Steady free convection flow within a tilted nanofluid saturated porous cavity in the presence of a sloping magnetic field energized by an exothermic chemical reaction administered by Arrhenius kinetics. International Journal of Heat and Mass Transfer, 129, 198–211.

[14] Khan N., Hossam A. N., Hashmi M. S., Khan S. U., & Tlili I. A. (2020). Theoretical analysis for mixed convection flow of Maxwell fluid between two infinite isothermal stretching disks with heat source/sink. Symmetry, 12, 1–18.

[15] Nadeem S., Akhtar S., & Abbas N. (2020). Heat transfer of Maxwell base fluid flow of nanomaterial with MHD over a vertical moving surface. Alexandria Engineering Journal, 59, 1847–1856.

[16] Salawu S. O., Disu A. B., & Dada M. S. (2020). On criticality for a generalized Couette flow of a branch-chain thermal reactive third-grade fluid with Reynolds viscosity model. Scientific World Journal, 20, 1–10.

[17] Jawad M., Shah Z., Islam S., Majdoubi J., Tlili I., Khan W., & Khan I. (2019). Impact of nonlinear thermal radiation and viscous dissipation on unsteady three-dimensional rotating flow of single-wall carbon nanotubes with aqueous suspensions. Symmetry, 11, 207–225.

[18] Shamshuddin M. D., Rajput G. R., Mishra S. R., & Salawu S. O. (2023). Radiative and exponentially space-based thermal generation effects on an inclined hydromagnetic aqueous nanofluid flow past thermal slippage saturated porous media. International Journal of Modern Physics B, 23, 2350202.

[19] Waqas H., Khan S. U., Shehzad S. A., & Imran M. (2019). Radiative flow of Maxwell nanofluid containing gyrotactic microorganism and energy activation with convective Nield conditions. Heat Transfer Asian Research, 48, 1663–1687.

[20] Acharya N., Maity S., & Kundu P. K. (2020). Differential transformed approach of unsteady chemically reactive nanofluid flow over a bidirectional stretched surface in the presence of magnetic field. Heat Transfer, 49, 3917–3942.

[21] Azama M., Xu T., Shakoor A., & Khan M. (2020). Effects of Arrhenius activation energy in development of covalent bonding in axisymmetric flow of radiative-Cross nanofluid. International Communications in Heat and Mass Transfer, 113, 104547.

[22] Mustafa M., Khan J. A., Hayat T., & Alsaedi A. (2017). Buoyancy effects on the MHD nanofluid flow past a vertical surface with chemical reaction and activation energy. International Journal of Heat and Mass Transfer, 108, 1340–1346.

[23] Salawu S. O., Oderinu R. A., & Ohaegbue A. D. (2021). Current density and thermodynamic analysis of energy optimization for double exothermic reaction of magneto-Oldroyd 8-constant material. Journal of King Saud University Science, 33, 101374.

[24] Dhlamini M., Mondal H., Sibanda P., & Motsa S. (2020). Activation energy and entropy generation in viscous nanofluid with higher order chemically reacting species. International Journal of Ambient Energy, 14, 1–13.

[25] Hayat T., Ullah I., Waqas M., & Alsaedi A. (2019). Attributes of activation energy and exponential-based heat source in flow of Carreau fluid with cross-diffusion effects. Journal of Non-Equilibrium Thermodynamics, 49, 1–10.

[26] Salawu S. O., & Okoya S. S. (2021). On criticality for a branched-chain thermal reactive-diffusion in a cylinder. Combustion Science and Technology, 192, 1–16.

[27] Dawar A., & Acharya N. (2022). Unsteady mixed convective radiative nanofluid flow in the stagnation point region of a revolving sphere considering nanoparticle diameter and nanolayer effects. Journal of Indian Chemical Society, 99, 100716.

[28] Kumar G. K., Ramesh G. K., Gireesha B. I., & Rashad A. M. (2019). On stretched magnetic flow of Carreau nanofluid with slip effects and nonlinear thermal radiation. Nonlinear Engineering, 8, 340–349.

[29] Okedoye A. M., Salawu S. O., & Asibor E. A. (2021). A convective MHD double diffusive flow of a binary mixture through an isothermal and porous moving plate with activation energy. Computational Thermal Sciences, 13, 45–60.

[30] Olanrewaju A. M., Salawu S. O., Olanrewaju P. O., & Amoo S. A. (2021). Unsteady radiative MHD flow and entropy generation of Maxwell nanofluid in porous media with Arrhenius chemical kinetics. Cogent Engineering, 8, 1942639.

[31] Makinde O. D. (2005). Free convection flows with thermal radiation and mass transfer past a moving vertical porous plate. International Communications in Heat and Mass Transfer, 32, 1411–1419.